J Mater Sci (2009) 44:4466–4471
DOI 10.1007/s10853-009-3677-3

Synthesis, characterization, and electrochemical properties of $Ni(OH)_2$/ultra-stable Y zeolite composite

Jun-Wei Lang · Ling-Bin Kong · Wei-Jin Wu · Yong-Chun Luo · Long Kang

Received: 10 February 2009 / Accepted: 9 June 2009 / Published online: 23 June 2009

Abstract A novel composite of $Ni(OH)_2$/ultra-stable Y zeolite materials was synthesized by an improved chemical precipitation method, which used the ultra-stable Y zeolite as the template. The $Ni(OH)_2$/ultra-stable Y zeolite composite and its microstructure were characterized by X-ray diffraction measurements and transmission electron microscopy. Electrochemical studies were carried out using cyclic voltammetry, chronopotentiometry technology and ac impedance spectroscopy, respectively. The result shows that the loose-packed whisker $Ni(OH)_2$ phase has profound impacts on electrode performance at very high power output. A maximum discharge capacity of 185.6 mA-h/g (1670 F/g), or 371 mA-h/g (3340 F/g) after correcting for weight percent of nickel hydroxide phase at the current density of 625 mA/g could be achieved in a half-cell setup configuration for the $Ni(OH)_2$/ultra-stable Y zeolite electrode, suggesting its potential application in electrode material for secondary batteries and electrochemical capacitors. Furthermore, the effect of NH_4Cl concentration on the electrochemical properties characteristics has also been systemically explored.

J.-W. Lang · L.-B. Kong (✉) · W.-J. Wu
State Key Laboratory of Gansu Advanced Non-ferrous Metal Materials, Lanzhou University of Technology, Lanzhou 730050, People's Republic of China
e-mail: konglb@lut.cn

Y.-C. Luo · L. Kang
Key Laboratory of Non-ferrous Metal Alloys and Processing of Ministry of Education, Lanzhou University of Technology, Lanzhou 730050, People's Republic of China

Introduction

Nickel hydroxide is widely studied for more than several decades, due to its application as positive electrodes of several primary and secondary alkaline batteries. $Ni(OH)_2$ continues to attract an attention because of the commercial importance of nickel based secondary batteries such as metal hydride-nickel (MH-Ni), cadmium-nickel (Cd-Ni), ferrum-nickel (Fe-Ni), and zinc-nickel (Zn-Ni) alkaline rechargeable batteries [1–4]. Novel structural and electrochemical properties of nickel hydroxide not only lift it to contribute in the battery application but also in the electrochemical capacitors [5–10].

Up to now, many groups have reported the preparation of different morphologies of $Ni(OH)_2$, such as nanorods [11], boardlike nanostructures [12], nanowires [13], and hollow spheres [14, 15]. As the physical and electrochemical characteristics of nickel hydroxide are the key to the properties of the electrodes, reduction in the size of the material has recently gained a considerable amount of attention which revolutionized their unique physical and chemical properties, because of their large surface to volume ratio. Nanostructured nickel hydroxide materials become important in the field of secondary batteries and electrochemical capacitors because they have high specific surface area, fast redox reactions, and shortened diffusion path in solid phase [16, 17].

There are several methods used to prepare nickel oxides such as chemical precipitation [18], electrodeposition [8], and sol–gel technique [9, 19]. Among these synthetic methods, chemical precipitation technique has one advantage over the others: it is a facile method. The sol–gel dip-coating method and cathodic precipitation method will inevitably encounter a serious fall in capacitance during scaling-up [20], the specific capacitance of device ranging

from 50 F/g to 696 F/g (for single-electrode system). Therefore, a lot of research work has been done to improve the electrochemical performance of nickel hydroxides. Nickel-based composites are one of the most commonly used candidates for secondary batteries and electrochemical capacitors, such as $Ni(OH)_2$/ultra-stable Y zeolite (USY) [7], NiO/SBA-15 [21], $Ni(OH)_2$/activated carbon [22].

In this study, a new intercalation compounds with loose-packed whisker $Ni(OH)_2$ phase have been synthesized by utilizing the ion-exchange properties of USY. Our strategy is to use a high surface area USY as the template on which the redox active inorganic nanostructure is synthesized through ion exchange, chemical precipitation, and self-directed growth processes. We demonstrate that the unique microstructure creates electrochemical accessibility of electrolyte OH^- ions to $Ni(OH)_2$ nano-whiskers and a fast diffusion rate within the redox phase. The maximum discharge capacity of 185.6 mA-h/g (1670 F/g), or 371 mA-h/g (3340 F/g) after correcting for weight percent of nickel hydroxide phase could be achieved for a single-electrode system, which shows better rate capability and great potential as the electrode materials for secondary batteries and electrochemical capacitors. In addition, the effect of NH_4Cl concentration on the electrochemical properties characteristics has also been systemically explored.

Experimental

Materials preparation

All of the chemicals were of analytical grade and used without further purification. USY was synthesized by repeated sodium exchange of zeolite NaY (LZPCC, Lanet-Y30, Si/Al = 4.56, BET surface area = 800 m^2/g) with aqueous solution of NH_4Cl at 86 °C for 1 h, followed by steaming at 540 °C for 2 h. The NH_4Cl concentrations were 0.5, 1.0, 1.5, 2.0, and 3.0 M, respectively. The obtained USY product was denominated sample $USY_{0.5}$, $USY_{1.0}$, $USY_{1.5}$, $USY_{2.0}$, and $USY_{3.0}$ corresponding to the different NH_4Cl concentration, respectively (without special denotation, the USY sample is referred to the NH_4Cl concentration of 2.0 M in this work).

The $Ni(OH)_2$/USY materials were synthesized by a liquid-precipitated method, which used the USY as the template. In the first step, nickel chloride hydrate solution (Ni concentration 1.5 M) was mixed in a glass beaker with a USY (6 wt%) water suspension using a magnetic stir bar. After 30 min, the mixed aqueous solution was slowly adjusted to pH 9 by dropwise addition of 5 wt% NH_4OH at a temperature of ~10 °C, control the addition time more than 2 h. The resulting suspension was stirred at this temperature for an additional 3 h. Then the solid was filtered, washed with a copious amount of distilled water, and dried at 100 °C in air for 6 h. Control the relative ratio of $NiCl_2 \cdot 6H_2O$ and the USY support in the starting mixture to make the weight percent of $Ni(OH)_2$ in composite is 50%.

Electrode preparation

The working electrodes were prepared according to the method reported in literature [23]. A total of 80 wt% of $Ni(OH)_2$/USY composite powder was mixed with 7.5 wt% of acetylene black (>99.9%) and 7.5 wt% of conducting graphite in an agate mortar until a homogeneous black powder was obtained. To this mixture, 5 wt% of poly (tetrafluoroethylene) was added with a few drops of ethanol. After briefly allowing the solvent to evaporate, the resulting paste was pressed at 10 MPa to a nickel gauze with a nickel wire for an electric connection. The electrode assembly was dried for 16 h at 80 °C in air. Each electrode contained about 8 mg of electroactive material and had a geometric surface area of about 1 cm^2.

Structure characterization

The obtained composites were characterized by transmission electron microscope (TEM) (JEOL, JEM-2010, Japan) and X-ray diffraction (XRD) measurements (Bruker, D8 Advance, Germany).

Electrochemical tests

Electrochemical measurements were carried out using an electrochemical working station (CHI660C, Shanghai, China) in a half-cell setup configuration at room temperature. A platinum gauze electrode and a saturated calomel electrode served as the counter electrode and the reference electrode, respectively. CV scans were recorded from 0.2 V to 0.6 V at different scan rate in 2 M KOH aqueous solution, and charge–discharge cycle tests were carried out in the potential range of 0 ~ 0.4 V in 2 M KOH aqueous solution at different constant current densities. Electrochemical impedance spectroscopy measurements were performed under open circuit potential in an ac frequency range from 10000 Hz to 0.01 Hz with an excitation signal of 5 mV. All electrochemical experiments were carried out at 20 ± 1 °C.

Results and discussion

Shown in Fig. 1 are the XRD patterns of the pure $Ni(OH)_2$ materials, pure USY, and the $Ni(OH)_2$/USY composite

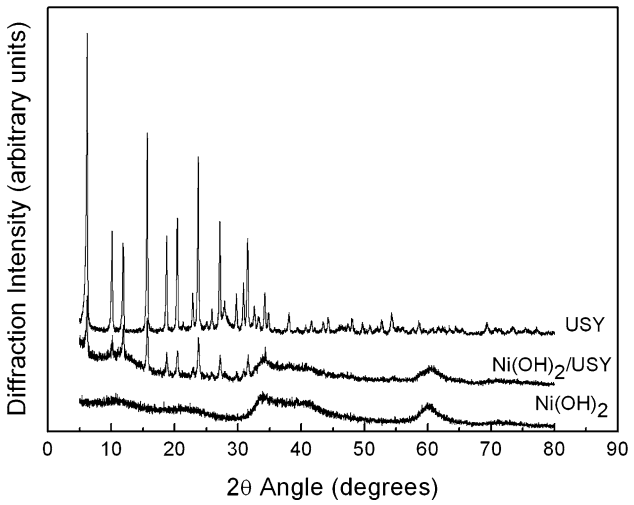

Fig. 1 XRD patterns of $Ni(OH)_2$, $Ni(OH)_2$/USY, and USY materials

material. No obvious peaks of β-nickel hydroxide have been observed in the XRD pattern of the as-prepared $Ni(OH)_2$ material, and it is correspond to the layered α-$Ni(OH)_2$ structure with low crystallinity [20]. From the curve of pure USY phase, it is noticed that the high and sharp diffraction peaks have occurred, which are directly linked to good crystallinity or larger crystal grain size. The diffraction patterns of the loaded $Ni(OH)_2$ electrochemical active material corresponding to that of pure USY had evidently changed. By contrast, the considerable broadening of diffraction peaks demonstrated that very small crystals of the synthesized $Ni(OH)_2$ material.

The morphology of as-prepared pure USY, $Ni(OH)_2$ material and the $Ni(OH)_2$/USY composite material was examined by TEM. As shown in Fig. 2a, pure USY has morphology of granular particles with a typical particle diameter of $\sim$500 nm. Figure 2b shows the morphologies of pure $Ni(OH)_2$ material, it is noteworthy that the network-like structure (which is consist of interconnected nano-flakes) shows anisotropic morphology characteristics and the formation of a loosely packed microstructure in the nanometer scale. Comparing Fig. 2a with c reveals that after USY is loaded with $Ni(OH)_2$, a salient morphology change has taken place on the outer surface of USY. The morphology of $Ni(OH)_2$/USY composite appears fuzzy in the TEM images. It is important to note that the whisker structure shows anisotropic morphology extending from the exterior of USY to interparticle open space, and

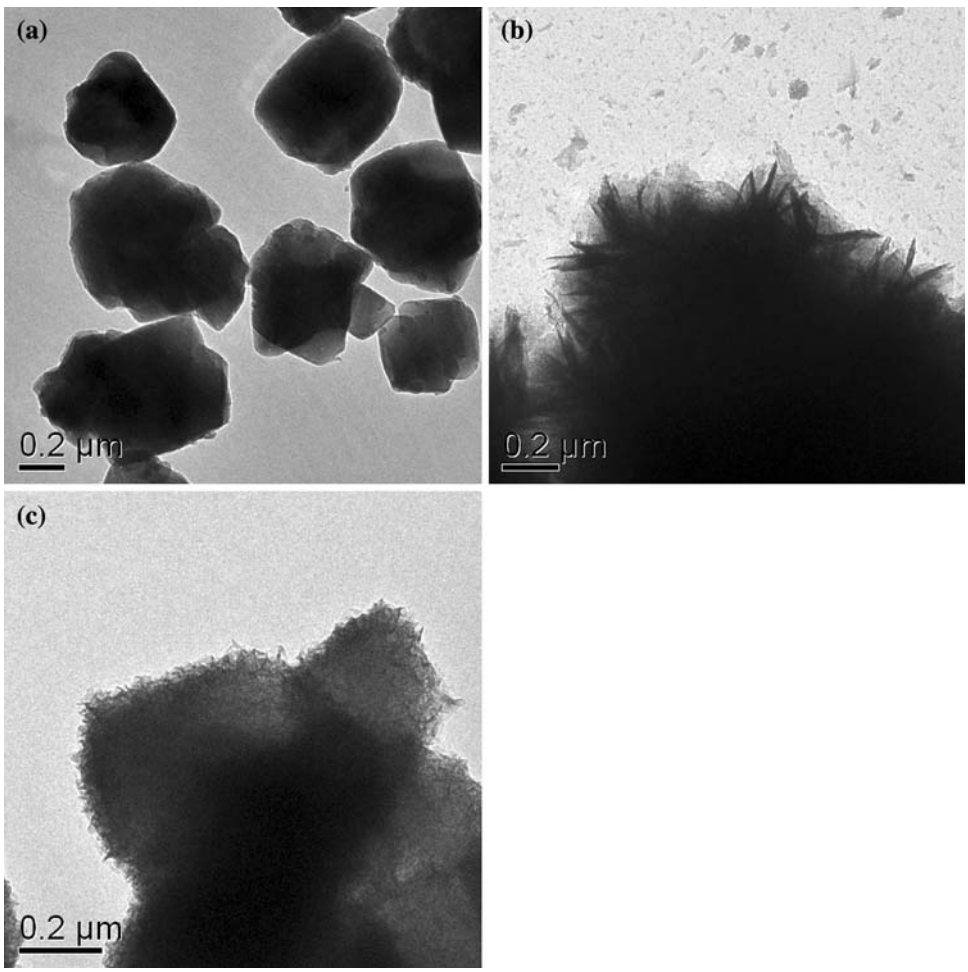

Fig. 2 TEM image of pure USY, pure $Ni(OH)_2$, and $Ni(OH)_2$/USY composite

forming a loosely packed microstructure sizing down to a few nanometers with ample space between adjacent whiskers. The unique structure plays a basic role in the morphology requirement for electrochemical accessibility of electrolyte OH^- to $Ni(OH)_2$ active material and a fast diffusion rate within the redox phase. It is believed that the unique structure provided an important morphological foundation for the extraordinary high discharge capacity and electrode performance at very high power output.

To evaluate the electrochemical properties of the prepared $Ni(OH)_2$/USY composite, cyclic voltammetry (CV) and chronopotentiometry measurements have been used and quantify the discharge capacity of the as-prepared $Ni(OH)_2$/USY composite electrode. Figure 3a shows the CV curves of the pure USY and $Ni(OH)_2$/USY composite. It was demonstrated that pure USY had negligible integral area under the current–potential response, suggesting USY alone with very small discharge capacity properties.

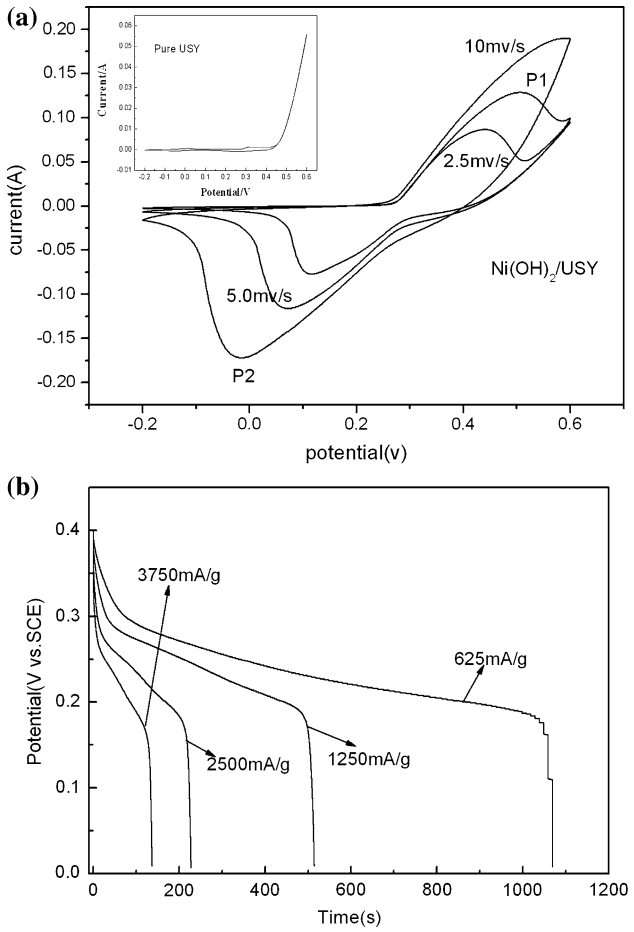

Fig. 3 Electrochemical properties of $Ni(OH)_2$/USY in the 2 M KOH solution: **a** CV curves at different scan rates within a potential window of −0.2 to 0.6 V vs. SCE, the inset is the CV curves of pure USY electrode; **b** discharging curves in the potential range from 0.4 V to 0 V at different discharging currents. The working electrode is 1 cm^2 containing about 8 mg $Ni(OH)_2$/USY

According to these observations, the $Ni(OH)_2$ phases of the composite are responsible for the main capacity. Furthermore, the shape of the CV curves of the $Ni(OH)_2$/USY composite reveals that the capacitance characteristic is very distinguished from that of electric double-layer capacitance in which the shape is normally close to an ideal rectangular shape. These indicate that the capacity mainly results from the pseudo-capacitance, which is based on a redox mechanism. It is well accepted that the surface faradic reactions will proceed according to the following reaction [7, 24]:

$$Ni(OH)_2 + OH \leftrightarrow NiOOH + H_2O + e^- \quad (1)$$

The two strong redox reaction peaks are responsible for the pseudo-capacitance, the anodic peak P1 is due to the oxidation of $Ni(OH)_2$ to NiOOH,and the cathodic peak P2 is for the reverse process. It should be noted that with the sweep rate increased, the shape of the CV changed, the anodic peak potential and cathodic direction, and the capacitance, inevitably, decreased, which is in agreement with the result of the chronopotentiometry measurement.

Figure 3b shows the discharging curves of the $Ni(OH)_2$/$USY_{2.0}$ electrode obtained in the potential range of 0–0.4 V in 2 M KOH at various current density. The discharge capacity and specific capacitance of the $Ni(OH)_2$/$USY_{2.0}$ electrode were calculated from $C_1 = I\Delta t/m$ (mA-h/g) and $C_2 = I/[(dE/dt) \times m] \approx I/[(\Delta E/\Delta t) \times m]$ (F/g), respectively, where I is the current density of discharge, dE/dt indicates the slope of the discharge plot of the discharging curves, and m is the mass of the corresponding electrode materials measured. In this way, the discharge capacities of the $Ni(OH)_2$/USY electrode at current densities of 625, 1250, 2500, and 3750 mA/g were 185.6, 178.8, 158, and 143.8 mA-h/g, or 371, 357.6, 316, and 287.6 mA-h/g after correcting for weight percent of nickel hydroxide phase, respectively. The specific capacitances of the $Ni(OH)_2$/USY electrode at current densities of 625, 1250, 2500, and 3750 mA/g were 1670, 1609, 1425, and 1294 F/g, or 3340, 3218, 2850, and 2588 F/g after correcting for weight percent of nickel hydroxide phase, respectively. It can be seen that the discharge capacity decreases as the current density increases as usual, but it still has more than 77.5% of the initial capacity at a discharge current density of as high as 3750 mA/g for $Ni(OH)_2$/USY electrode, so the excellent rate capability of the sample makes it attractive particularly for a practical application. Therefore, the loose-packed whisker $Ni(OH)_2$ phase has profound impacts on electrode performance at very high power output.

A series of $Ni(OH)_2$/USY materials were synthesized use different USY as the template. The obtained $Ni(OH)_2$/USY product was denominated $Ni(OH)_2$/$USY_{0.5}$, $Ni(OH)_2$/$USY_{1.0}$, $Ni(OH)_2$/$USY_{1.5}$, $Ni(OH)_2$/$USY_{2.0}$, and $Ni(OH)_2$/$USY_{3.0}$, corresponding to the sample $USY_{0.5}$, $USY_{1.0}$, $USY_{1.5}$, $USY_{2.0}$, and $USY_{3.0}$, respectively. Figure 4 shows

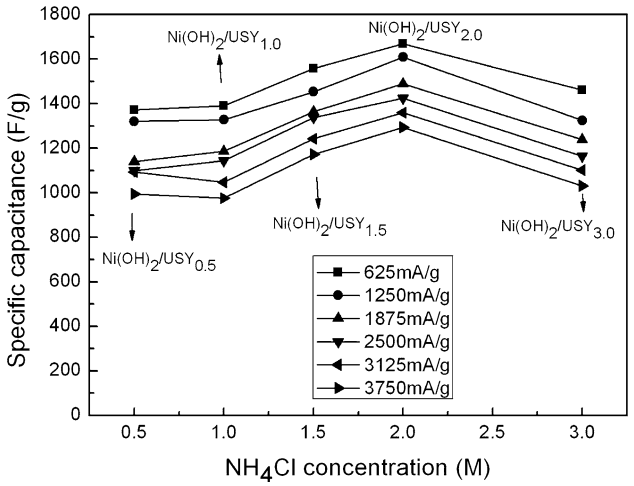

Fig. 4 The specific capacitance of $Ni(OH)_2$/USY materials prepared with different NH_4Cl concentration as a function of discharge currents. The working electrodes have a geometric area of 1 cm^2 and contain 8 mg of $Ni(OH)_2$/USY

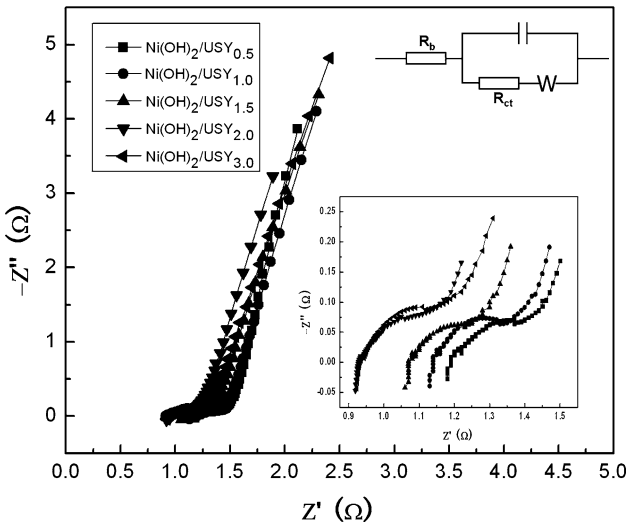

Fig. 5 Complex-plane impedance plot of the composite electrode prepared at different concentrations NH_4Cl ion exchange: 0.5, 1.0, 1.5, 2.0, and 3.0 M (0.27 V vs. SCE; electrolyte: 2.0 M KOH).The inset is the equivalent circuit and the high frequency regions

the effect of different NH_4Cl concentration on the capacitive properties of the $Ni(OH)_2$/USY electrodes. The specific capacitance of the composite increases almost linearly with increasing the NH_4Cl mass at low concentration, and reaches a maximum of 1670 F/g (185.6 mA-h/g) of the $Ni(OH)_2/USY_{2.0}$ electrodes. As the increases beyond 2.0 M, the specific capacitance of the composite decreased. The ascending and decline tendency of the specific capacitance is similar and relevant to different discharge currents.

The electrochemical impedance measurements were carried out on the $Ni(OH)_2$/USY electrodes at 0.318 V (vs. SCE). The typical results are shown in Fig. 5. The complex plane impedance plots for each sample can be divided into the high-frequency component and the low-frequency component. A distinct knee in the frequency can be observed in curves of Fig. 5. From the point intersecting with the real axis in the range of high frequency, the internal resistances (which equal to R_b) of the $Ni(OH)_2$/USY electrodes are shown in Table 1. It includes the total resistances of the ionic resistance of electrolyte, intrinsic resistance of active materials and contact resistance at the active material/current collector interface. This can be explained that with the increase of the NH_4Cl concentration, the increase in the Si/Al ratio and crystallinity can enhance the interaction of USY and $Ni(OH)_2$, to form a more loosely packed composite with a microstructure in the nanometer scale. The special microstructure can enhance the diffusivity of the electrolyte ions in the composite electrode. The semicircle in the high frequency range associates with the surface properties of porous electrode corresponds to the faradic charge-transfer resistance (R_{ct}). It can be seen that all the $Ni(OH)_2$/USY samples have small charge-transfer resistance. At the lower

Table 1 The internal resistances (which equal to R_b) of the $Ni(OH)_2$/USY electrodes

Sample	Open circuit potential (V)	R_b (Ω)
$Ni(OH)_2/USY_{0.5}$	0.318	1.18
$Ni(OH)_2/USY_{1.0}$	0.318	1.13
$Ni(OH)_2/USY_{1.5}$	0.318	1.06
$Ni(OH)_2/USY_{2.0}$	0.318	0.919
$Ni(OH)_2/USY_{3.0}$	0.318	0.923

frequencies, a straight sloping line represents the diffusive resistance (Warburg impendence) of the electrolyte in electrode pores and the proton diffusion in host materials. The phase angles for impedance plots of all the $Ni(OH)_2$/USY electrodes were observed to be higher than 45° in the low frequencies clearly. These findings suggest that all the electrodes are not controlled by diffusion process, implying the good accessibility of the ions and/or the possible contributions of electrochemical capacitors [25, 26].

The long-term electrochemical stability of the $Ni(OH)_2$/USY in 2 M KOH electrolyte has been examined by chronopotentiometry. As shown in Fig. 6 the cycling stability was tested over 1000 cycles. It exhibited a loss of 60% in capacitance during the 1000 cycles, indicates that the repetitive charge–discharges do induce noticeable degradation of the microstructure. The Nickel hydroxide crystallizes in two polymorphic modifications known as α and β. Consequently, the reversible reactions of nickel hydroxide, involve two redox couples, namely, the α-$Ni(OH)_2/\gamma$-NiOOH and the β-$Ni(OH)_2/\beta$-NiOOH. α-$Ni(OH)_2$ can be cycled to γ-NiOOH phase reversibly without any mechanical

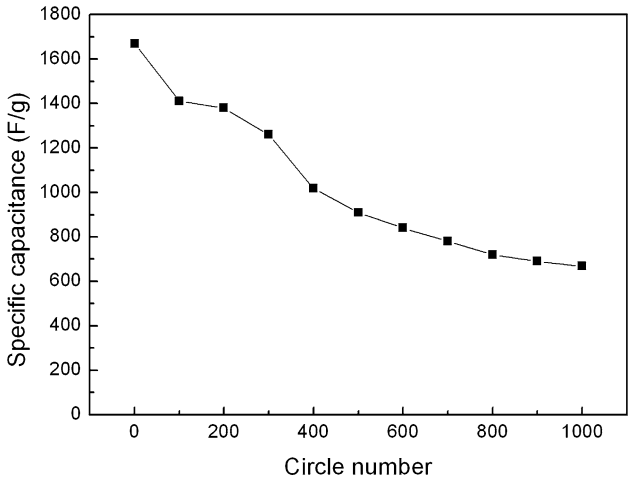

Fig. 6 Cycle life of as-prepared $Ni(OH)_2$/USY electrode at the discharge current of 625 mA/g in 2 M KOH electrolyte

deformation. Besides, a higher theoretical capacity for the nickel-positive electrode comprising α-$Ni(OH)_2$ is envisaged in relation to a β-$Ni(OH)_2$ electrode. However, α -$Ni(OH)_2$ happens to be unstable in alkaline medium and transforms to β-$Ni(OH)_2$, and the α/γ couple is rapidly aged to the β/β couple [6, 27, 28]. We have produce stabilized α-$Ni(OH)_2$ as electrode material since the presence of dissolved Al cations in alkaline electrolyte can suppress the $\alpha \rightarrow \beta$-nickel hydroxide transformation. The XRD result showed that α-$Ni(OH)_2$ without any Al has completely transformed to β-phase after ageing in 20 mL of 6 M KOH for 15 days at room temperature, so the capacitance fading may originate from the slow transformation of α-$Ni(OH)_2$ to β-$Ni(OH)_2$.

Conclusion

In summary, a new strategy for preparing materials with unique microstructures is described. A novel $Ni(OH)_2$/USY nanocomposite was successfully prepared using this strategy. The structure characterizations show that the as-prepared $Ni(OH)_2$/USY materials have a less crystallization, loosely packed nano-whiskers structure. The unique microstructure can accommodate the electroactive species in the solid bulk electrode material, and creates electrochemical accessibility of electrolyte OH^- ions and fast diffusion rate through bulk materials, which is fundamental for materials showing characteristics of electrochemical capacitors rather than general batteries. Consequently, a maximum discharge capacity of 185.6 mA-h/g (1670 F/g), or 371 mA-h/g (3340 F/g) after correcting for weight percent of nickel hydroxide phase is achieved for the $Ni(OH)_2/USY_{2.0}$ electrode. The effect of NH_4Cl concentration for USY on the electrochemical properties of $Ni(OH)_2$/USY composite was also been studied, it is shown that NH_4Cl concentration is a crucial factors in the improvement of the electrochemical properties of the composite. Even though we do not fully understand the growth mechanism of $Ni(OH)_2$ nano-whiskers, this novel technique is able to be extend to other transition metal oxides systems.

Acknowledgements This study is supported by the National Natural Science Foundation of China (No. 50602020), the Natural Science Foundation of Gansu Province (No. 0803RJZA002) and the Program for Outstanding Young Teachers in Lanzhou University of Technology (No. Q200803).

References

1. Wang XY, Yan J, Zhang YS, Yuan HT, Song DY (1998) J Appl Electrochem 28:1377
2. Buono-core GE, Tejos M, Alveal G, Hill RH (2000) J Mater Sci 35:4873. doi:10.1023/A:1004857720136
3. Lei LX, Hu M, Gao XR, Sun YM (2008) Electrochim Acta 54:671
4. Kuma VG, Munichandraiah N, Kamath PV, Shukla AK (1995) J Power Sources 56:111
5. Lang JW, Kong LB, Wu WJ, Luo YC, Kang L (2008) Chem Commun 35:4213
6. Lang JW, Kong LB, Wu WJ, Liu M, Luo YC, Kang L (2009) J Solid State Electrochem 13:333
7. Cao L, Kong LB, Liang YY, Li HL (2004) Chem Commun 14:1646
8. Srinivasan V, Weidner JW (1997) J Electrochem Soc 144:L210
9. Cheng J, Cao GP, Yang YS (2006) J Power Sources 159:734
10. Wu MS, Huang YA, Yang CH, Jow JJ (2007) Int J Hydrogen Energy 32:4153
11. Yang DN, Wang RM, He MS, Zhang J, Liu ZF (2005) J Phys Chem B 109:7654
12. Chen DL, Gao L (2005) Chem Phys Lett 405:159
13. Wang Y, Zhu QS, Zhang HG (2005) Chem Commun 41:5231
14. Li YM, Li WY, Chou SL, Chen J (2008) J Alloys Compd 456:339
15. Wang DB, Song CX, Hu ZS, Fu X (2005) J Phys Chem B 109:1125
16. Wu MS, Hsieh HH (2008) Electrochim Acta 53:3427
17. Barakat NAM, Omran AEM, Aryal S, Sheikh FA, Kang HK, Kim HY (2008) J Mater Sci 43:860. doi:10.1007/s10853-007-2190-9
18. Song QS, Li YY, Lchan SL (2005) J Appl Electrochem 35:157
19. Liu KC, Anderson MA (1996) J Electrochem Soc 143:124
20. Xing W, Li F, Yan ZF, Lu GQ (2004) J Power Sources 134:324
21. Wang YG, Xia YY (2006) Electrochim Acta 51:3223
22. Huang QH, Wang XY, Li J, Dai CL, Gamboa S, Sebastian PJ (2007) J Power Sources 164:425
23. Cao L, Lu M, Li HL (2005) J Electrochem Soc 152:A871
24. Vazquez MV, Avena MJ, Pauli CP (1995) Electrochim Acta 40:907
25. Xu MW, Bao SJ, Li HL (2007) J Solid State Electrochem 11:372
26. Zhang SS, Xu K, Jow TR (2004) Electrochim Acta 49:1057
27. Kamath PV, Dixit M, Indira L, Shukla AK, Kumar VG, Munichandraiah N (1994) J Electrochem Soc 141:2956
28. Jayashree RS, Kamath PV (2001) J Appl Electrochem 31:1315